

# Highly efficient deep-blue fluorescent dopant for achieving low-power OLED display satisfying BT.2020 chromaticity

Yusuke Takita 

Kyoko Takeda

Naoaki Hashimoto

Shiho Nomura

Tsunenori Suzuki

Harue Nakashima

Shogo Uesaka

Satoshi Seo

Shunpei Yamazaki (Permanent Member)

**Abstract** — In this work, novel blue-fluorescent dopants with a heteroaromatic ring skeleton instead of the conventional pyrene skeleton were investigated. Bottom-emission organic light-emitting diodes (OLEDs) fabricated using the novel blue-fluorescent dopants in light-emitting layers achieved better deep-blue chromaticity than OLEDs based on a conventional pyrene-based dopant, while maintaining both high external quantum efficiency (EQE) and comparable reliability. The attainment of deep-blue chromaticity without losing high EQE was ascribed to the improvement of the efficiency of energy transfer from the host to the dopant. Furthermore, it was estimated that using this novel dopant in a top-emission OLED panel that satisfies BT.2020 chromaticity enables the power consumption of the whole panel to be 24% lower than that of the panel with a conventional dopant.

**Keywords** — OLED, fluorescent OLED, deep blue, BT.2020 color gamut.

DOI # 10.1002/jsid.634

## 1 Introduction

Since a first report of a highly efficient organic light-emitting diode (OLED) with a heterostructure in 1987, OLEDs have been actively researched for use in various light-emitting devices.<sup>1</sup> In particular, OLED displays have attracted intensive attention as potential replacements for liquid-crystal displays. In recent years, one of the major targets for the development of OLED displays has been focused on 8 K displays. 8 K displays have a very high resolution of 7680 × 4320 and employ the BT.2020 standard as a color gamut standard.<sup>2</sup> The most important feature of the BT.2020 standard is 99.9% reproducibility of colors in nature, and it satisfies a drastically wider color gamut than the conventional standard red, green, and blue (sRGB) standard.<sup>3</sup> A light-emitting material with better chromaticity is needed to achieve this wide color gamut. Of course, in addition to good chromaticity, high efficiency and a long lifetime are also required.

In terms of obtaining an OLED that satisfies wide color gamut with maintaining high efficiency and a long lifetime, the most difficult subject is the development of a blue OLED among red, green, and blue ones. In recent years, many trials towards the realization of highly efficient blue OLEDs based on phosphorescence<sup>4–6</sup> and thermally activated delayed fluorescence (TADF)<sup>7–9</sup> have been reported. Because both phosphorescent and TADF OLEDs are assumed to achieve 100% internal quantum efficiency in principle, high efficiency is expected also in blue OLEDs. However, they require a high excited triplet (T1) energy, which makes obtaining light emission with deep-blue

chromaticity extremely difficult. Actually, most blue phosphorescent and blue TADF OLEDs emit light with broad emission spectra, and emission of BT.2020 deep-blue light has never been attained. Moreover, the reliability of existing devices with blue phosphorescence or TADF is insufficient, and such devices have not yet reached the level of practical use. Therefore, only the fluorescent OLEDs have been used as practical blue-light-emitting devices in OLED displays.

Fluorescent OLEDs have been known to exhibit excellent reliability. In addition, they are favorable for obtaining deep-blue light emission, because their emission spectra are sharp compared with phosphorescent OLEDs and TADF OLEDs. The most serious drawback in fluorescent OLEDs, however, is their limited internal quantum efficiency of 25% due to the spin selection rule in principle. Utilizing triplet-triplet-annihilation (TTA) mechanism, some of non-emissive triplet excitons produced by carrier recombination can be upconverted into emissive singlet excitons, enabling the theoretical internal quantum efficiency limit of 25% to be overcome.<sup>10–12</sup> Previously, we reported highly efficient blue-fluorescent OLEDs using TTA.<sup>13–15</sup> Combining the TTA mechanism with an efficient blue-fluorescent dopant with a pyrene skeleton, we achieved a maximum external quantum efficiency (EQE) of 12.7%, which is extremely high for fluorescent OLEDs.

However, the EQE of blue-light-emitting OLEDs with a fluorescent dopant with the conventional pyrene skeleton tended to become lower, when the molecular structure of the fluorescent dopant with a pyrene skeleton was modified for the improvement of blue chromaticity. We reported an

Received 02/16/18; accepted 02/26/18.

The authors are with the Semiconductor Energy Laboratory Co., Ltd., 398 Hase, Atsugi-shi, Kanagawa 243-0036, Japan; e-mail: yt1314@sel.co.jp.

© 2018 The Authors. *Journal of the Society for Information Display* published by Wiley Periodicals, Inc. on behalf of Society for Information Display 1071-0922/18/2602-0634\$1.00.

This is an open access article under the terms of the Creative Commons Attribution-NonCommercial License, which permits use, distribution and reproduction in any medium, provided the original work is properly cited and is not used for commercial purposes.

excellent deep-blue dopant, BD-02, a pyrene-based fluorescent dopant that exhibited BT.2020 blue light ( $x = 0.131$ ,  $y = 0.046$ ) in a top-emission OLED in our previous work.<sup>16</sup> However, the EQE of the bottom-emission device with BD-02 was as high as 10.7%. Therefore, utterly new design of blue fluorescent dopants for TTA-type blue OLEDs is necessary.

In the present study, we developed novel dopants with a heteroaromatic ring skeleton instead of a pyrene skeleton. Compared with OLEDs with BD-02, a conventional pyrene-based deep-blue dopant, OLEDs with our novel dopants emit deep-blue light with maintaining high EQE. Moreover, by incorporating a microcavity structure, the efficiencies of top-emission devices using the novel dopants were 1.7 times higher than that of the device using BD-02 at the BT.2020 blue chromaticity. Our estimation revealed that the power consumption of OLED display panels using the novel dopants is markedly lowered.

## 2 Novel deep blue dopants

### 2.1 Light-emitting characteristics of dopants

First, the emission characteristics of the new dopants were compared with those of BD-02. Figure 1 compares the photoluminescence (PL) spectra of our blue dopants, BD-02, BD-05, and BD-06 in toluene solutions. BD-02 has a peak at 450 nm, indicating that an OLED device containing BD-02 along with a microcavity structure satisfies BT.2020 blue emission. The EQE of this OLED, however, is not high enough, even though TTA mechanism is assumed to contribute to the increase of EQE. We developed two dopants, BD-05 and BD-06, each with a heteroaromatic ring skeleton different from a pyrene skeleton. The two dopants have the same skeletal luminophore but show some differences in PL spectra. Change of a substituent attached to the heteroaromatic skeleton is effective for the shift of PL spectra. The PL spectra of BD-05 and BD-02 have peaks at similar locations (448 and 450 nm, respectively), while the peak in the spectrum of BD-06 is located at a

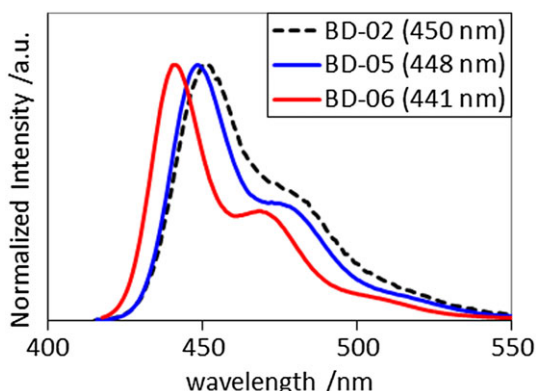


FIGURE 1 — Photoluminescence (PL) spectra of BD-02, BD-05, and BD-06 in toluene solutions (values of peaks are shown in parentheses).

shorter wavelength (441 nm). It should be also noted that the shoulder peaks of BD-05 and BD-06 are less intense than that of BD-02, and the main peaks of the new dopants are sharper than that of BD-02. These spectral features indicate that the novel materials should be effective for obtaining deep-blue light emission when used in devices with microcavity structures.

Table 1 shows the PL quantum yields (PLQYs) of the dopants in toluene solutions. The PLQY of BD-02 was 91%, whereas those of BD-05 and BD-06 were 93% and 97%, respectively, and higher than that of BD-02. This indicates that BD-05 and BD-06 are excellent blue dopants with high PLQYs, in addition to sharper spectra at shorter peak wavelength.

Table 2 shows the values of the HOMO and LUMO levels of the dopants. These values were estimated from the cyclic voltammetry measurements.<sup>17</sup>

### 2.2 Device characteristics

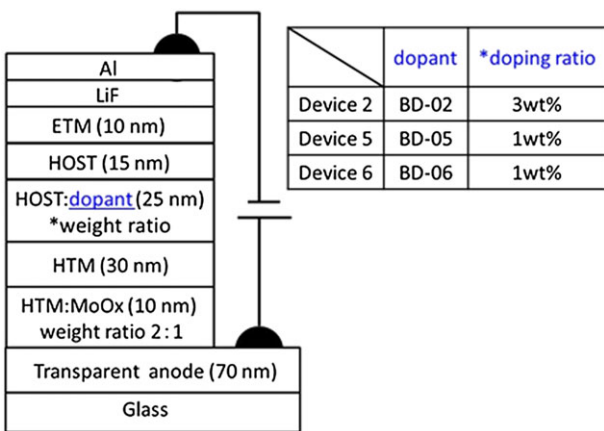
Bottom-emission devices (Devices 5 and 6) were fabricated using BD-05 and BD-06, respectively. Device 2 using BD-02 was also fabricated for reference. These devices were fabricated by vacuum evaporation, and all the devices had the same structures except for emissive dopants as is shown in Fig. 2. The doping ratio of Devices 5 and 6 is 1%, which is smaller than that of Device 2, because the reliabilities of Devices 5 and 6 were the best at this doping ratio. Since the efficiency of energy transfer from the host to BD-05 and BD-06 are higher than that from the host to BD-02 as is discussed in Sections 2–3, high EQEs can be obtained despite small doping ratio of BD-05 and BD-06. Figures 3 and 4 show the molecular structures of the materials and their energy level diagram, respectively. Drive voltages of these devices were quite low as is shown later. This originates from the use of our specific hole injection layer/hole transport layer (HIL/HTL) combination. A mixed layer of an organic material and molybdenum oxide is formed via co-deposition of a hole-transport material (HTM) and molybdenum oxide ( $\text{MoO}_3$ ), and used for HIL. This is

TABLE 1 — Photoluminescence quantum yields (PLQYs) of the novel dopants (BD-05 and BD-06) and a conventional dopant (BD-02) in toluene solutions.

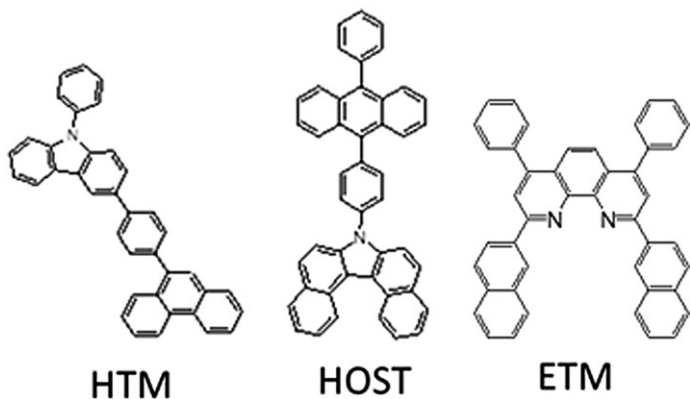
	BD-02	BD-05	BD-06
PLQY /%	91	93	97

TABLE 2 — The values of the HOMO and LUMO levels of novel dopants and a conventional dopant as calculated from the results of cyclic voltammetry measurements.

	BD-02	BD-05	BD-06
HOMO /eV	−5.45	−5.41	−5.48
LUMO /eV	−2.66	−2.66	−2.68



**FIGURE 2** — Device structures of the bottom-emission devices using BD-02, BD-05, and BD-06 (Devices 2, 5, and 6).\*MoO<sub>x</sub>:  $2 < x < 3$ . MoO<sub>3</sub> is used as an evaporation source and its composition changes during evaporation because of heat-induced deoxidization.



**FIGURE 3** — Molecular structures of the materials.

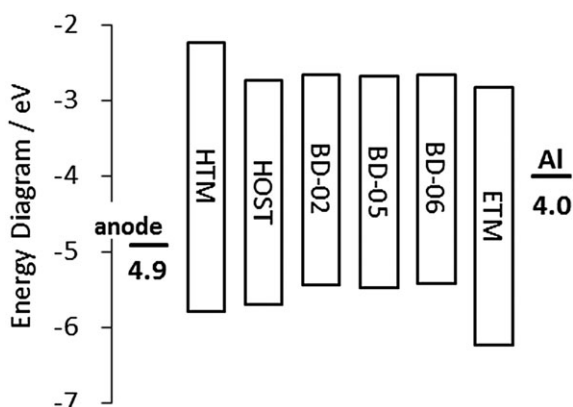


**FIGURE 4** — Energy level diagram of the materials used in the bottom-emission devices.

our original HIL and is called an organic hole-transport material/molybdenum oxide composite (OMOx). When the same HTM is used both for HTL and OMOx (HIL), as illustrated in Fig. 2, HIL forms ohmic contacts with HTL and an indium-tin-silicon-oxide anode [ITSO; indium tin oxide (ITO) containing SiO<sub>2</sub>].<sup>18–21</sup> That is, holes are easily injected from ITSO into HTL via HIL.

Figures 5 and 6 compare the electroluminescence (EL) spectra and EQEs of three devices, respectively. The EL spectrum of Device 5 has a peak at 457 nm, which substantially overlaps with that of Device 2. The EL peak of Device 6 locates at a shorter wavelength (451 nm) than that of Device 2. It should be noted that the emission wavelengths of Devices 5 and 6 using our novel dopants are short enough to satisfy the chromaticity coordinates of the BT.2020 blue color, when an optimized microcavity structure is incorporated into the devices. The EQEs of Devices 5 and 6 at approximately 1000 cd/m<sup>2</sup> are 11.8% and 11.4%, respectively, and higher than that of Device 2 (10.7%). As is shown in Table 1, the PLQYs of BD-05 and BD-06 are little bit higher than that of BD-02. This small difference in PLQY, however, does not give reason for the large difference in efficiency between devices (in particular, between Devices 2 and 5).

One of the reasons why the efficiencies of Devices 5 and 6 are higher than that of Device 2 is considered to be the difference of molecular orientation. Therefore, the anisotropic factor ( $a$ ) of each dopant was evaluated according to the published literatures.<sup>22–24</sup> The anisotropic factor  $a$  is 0.33 when the dipole orientation is isotropic and becomes 0 when the dipole orientation becomes perfectly parallel to the substrate. The anisotropic factor  $a$  of BD-02

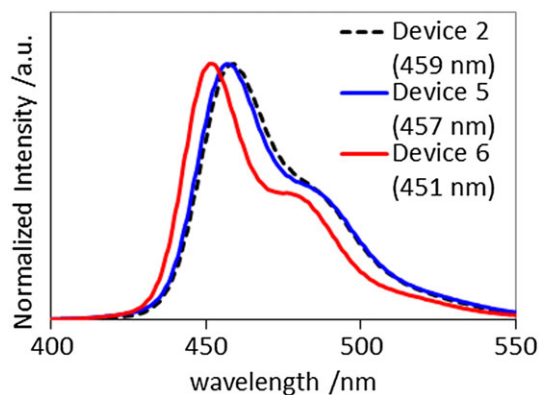


**FIGURE 5** — Electroluminescence (EL) spectra of Devices 2, 5, and 6 (values of peaks are shown in parentheses).

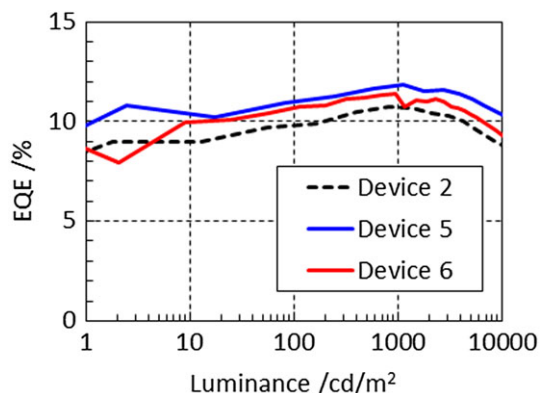


**FIGURE 6** — External quantum efficiencies (EQEs) of Devices 2, 5, and 6.

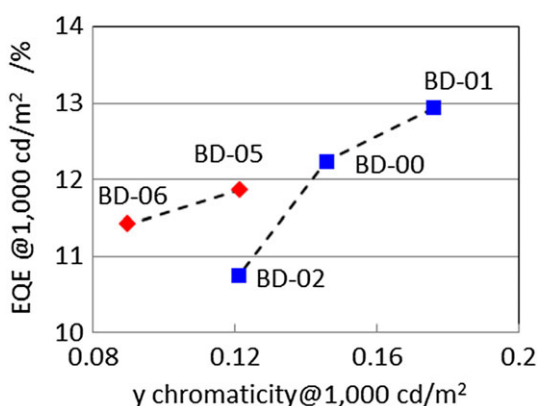
was estimated to be 0.23, whereas those of BD-05 and BD-06 were estimated to be 0.18 and 0.13, respectively. These results suggest that BD-05 and BD-06 have horizontal orientations and enhance the outcoupling efficiency compared to BD-02, which probably affects the higher efficiencies of Devices 5 and 6 than that of Device 2.

In addition, we assume that the efficiency of energy transfer from singlet excitons of host molecules to those of guest molecules may be the major origin of the difference of EQEs. In other words, the high EQEs of Devices 5 and 6 are explained by higher efficiency of energy transfer from the host to BD-05 and BD-06 than that from the host to BD-02. The details are described in Section 2–3.

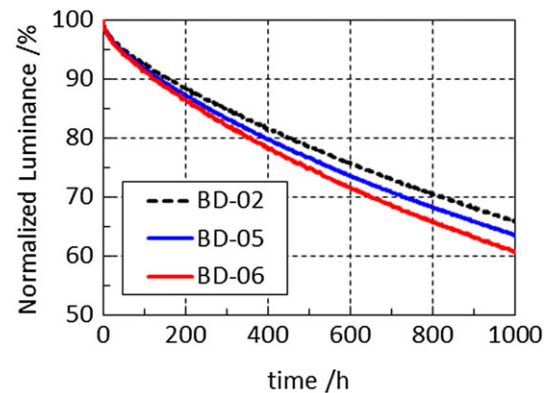
Figure 7 shows the correlations between the  $y$  chromaticity and EQE of the bottom-emission devices fabricated using the different dopant materials. In Fig. 7, the data of dopants (BD-00 and BD-01), each of which has the same pyrene skeleton as that of BD-02 and emits light with a longer wavelength than that of BD-02, are added. As the  $y$  chromaticity improved, the EQEs of the devices based on BD-00, BD-01, and BD-02, which are conventional pyrene-based dopants, decreased significantly, and the EQE of the deep-blue dopant BD-02 dropped down to less than 11%. In contrast, BD-05 and BD-06 retained high efficiency, even when  $y$  chromaticity shifted to deep blue.

Figure 8 shows the normalized luminance decay curves of the devices driven at a constant current density ( $50 \text{ mA/cm}^2$ ). The 10% luminance decay time (LT90) values of Devices 5 and 6 were 140 and 125 h, respectively. These LT90 values are nearly comparable with that of Device 2 (150 h).

Table 3 lists the major device characteristics at approximately  $1000 \text{ cd/m}^2$ . Devices based on BD-05 and BD-06 demonstrated high efficiency, while the chromaticity of BD-05 was essentially equal to that of BD-02, whereas the chromaticity of BD-06 was better than that of BD-02. It is worth emphasizing that three major requirements, deep-blue chromaticity, high efficiency, and high durability are all satisfied in Devices 5 and 6 using our novel dopants, BD-05 and BD-06.



**FIGURE 7** — Correlations between  $y$  chromaticity and EQE for devices based on conventional pyrene-based dopants (BD-00, BD-01, and BD-02) and novel dopants with heteroaromatic ring skeletons (BD-05 and BD-06).



**FIGURE 8** — Normalized luminance decay curves of Devices 2, 5, and 6 driven at a constant current density ( $50 \text{ mA/cm}^2$ ).

### 2.3 Energy transfer from host to dopant

In this section, the factor contributing to the higher efficiencies of Devices 5 and 6 relative to that of Device 2 is considered in terms of energy transfer from the host to the dopant. For energy transfer from a host to a dopant via the Förster mechanism, the rate constant  $k^{H \rightarrow G}$  of the energy transfer is expressed by Eq. (1)<sup>25</sup>:

$$k^{H \rightarrow G} = \frac{9000c^4 \ln 10}{128\pi^5 n^4 N_A \tau_0^H} \cdot \frac{k^2}{r^6} \int f_H(v) \varepsilon_G(v) \frac{dv}{v^4} \quad (1)$$

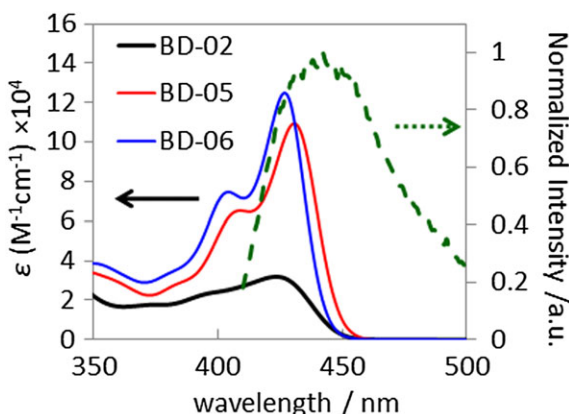
where  $c$ ,  $n$ ,  $\tau_0^H$ ,  $N_A$ , and  $k^2$  represent the speed of light, a refractive index of a medium, the natural radiation lifetime of the host, Avogadro's number, and an orientation factor, respectively.  $v$  represents a wavenumber, and  $r$  represents distance between a host molecule and a dopant molecule. In addition,  $f_H(v)$  represents a shape function of an emission spectrum of the host, and  $\varepsilon_G(v)$  represents the molar absorption coefficient of the dopant. The integral term of Eq. (1) shows that the rate constant of the energy transfer increases with increasing overlap between the emission spectrum of the host and the molar-absorptivity spectrum of the dopant.

Figure 9 shows the PL spectrum of the host (a 50-nm-thick thin film) and the absorption spectrum of each dopant in a toluene solution (the vertical axis represents the molar absorption coefficient). Our original material, the structure is shown in Fig. 3, was used as the host material. The PL spectrum of the host is in arbitrary scale, but the vertical axis of the absorption spectra of the dopants is scaled by a molar absorption coefficient ( $\text{M}^{-1} \text{ cm}^{-1}$ ).

Although the emission wavelength of BD-05 is substantially the same as that of BD-02 as shown in Fig. 1, marked difference between the absorption spectra of BD-02 and BD-05 was found. BD-05 has an absorption peak at a longer wavelength than that of BD-02 and has a higher molar absorption coefficient than BD-02. Thus, the overlap between the emission spectrum of the host and the absorption spectrum of BD-05 is larger than the overlap

**TABLE 3** — Device characteristics of Devices 2, 5, and 6 at approximately 1000 cd/m<sup>2</sup>.

Voltage (V)	Current density (mA/cm <sup>2</sup> )	Chromaticity		Current efficiency (cd/A)	EQE (%)	LT90 (h) (@50 mA/cm <sup>2</sup> )
		x	y			
Device 2	3.10	7.77	0.140	0.121	10.4	10.7
Device 5	3.10	9.60	0.140	0.122	11.6	11.8
Device 6	3.10	10.2	0.141	0.090	9.15	11.4

**FIGURE 9** — An overlap between a PL spectrum (broken curve) of a host (thin film) and an absorption spectrum (solid curve) of each dopant in a toluene solution. The PL spectrum of the host is in arbitrary scale, and the vertical axis is scaled by a molar absorption coefficient  $\epsilon$  ( $M^{-1} \text{ cm}^{-1}$ ) of the absorption spectrum of the dopant.

between the emission spectrum of the host and the absorption spectrum of BD-02. This difference in overlap implies that the rate of energy transfer from the host to BD-05 is higher than that to BD-02, resulting in a higher EQE of BD-05 than that of BD-02.

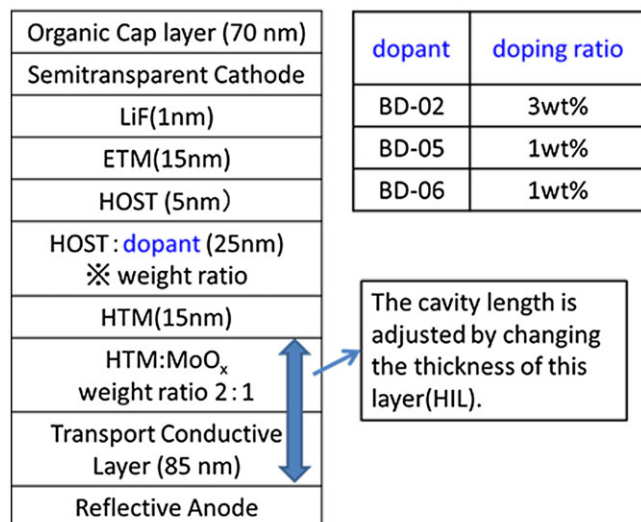
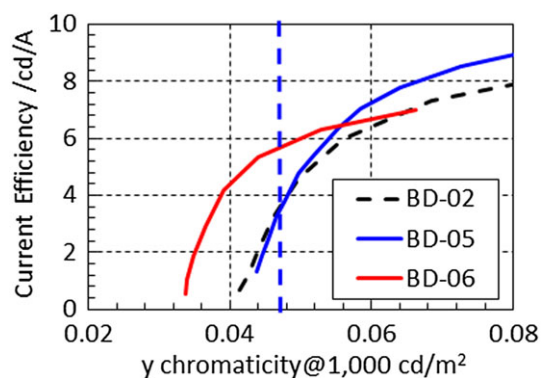
By contrast, the peak wavelength in the absorption spectrum of BD-06 is substantially the same as that of BD-02, whereas the molar absorption coefficient of BD-06 is much larger than that of BD-02. Therefore, it is assumed that the rate of energy transfer from the host to BD-06 is higher than that to BD-02 but lower than that to BD-05. This order of the rate of the energy transfer, we examined here, well corresponds to the EQE of the devices, and this facts give a rationale for the influence of the rate of energy transfer on EQE in our dopant/host system.

We conclude that, in the design of a dopant/host system for obtaining high efficiency deep-blue-fluorescent OLEDs, increasing the molar absorption coefficient of a dopant and increasing the overlap between the emission spectrum of a host and the absorption spectrum of a dopant are key issues.

### 3 Device optimization for OLED displays satisfying BT.2020 standard

Top-emission devices with microcavity structure were fabricated to obtain blue light satisfying the BT.2020

standard. The microcavity structure increases the intensity of light of a specific wavelength and allows the light to be extracted via the optical resonance effect between electrodes. Top-emission devices based on essentially the same device structure with the bottom-emission devices were fabricated as shown in Fig. 10. In these devices, the thicknesses of HILs (OMOx) were varied to change the optical resonance wavelength. Because our original OMOx shows no absorption in the visible region,<sup>26</sup> the emission efficiency is not influenced by the film thickness of HIL, even when the

**FIGURE 10** — Structures of the top emission devices with microcavity structures.**FIGURE 11** — Relationships between  $y$  chromaticity and current efficiency when a microcavity structure is used in the top-emission devices based on BD-02, BD-05, and BD-06 (the blue dashed line in the graph shows the  $y$  chromaticity of the BT.2020 standard [ $y = 0.046$ ]).

thickness of the OMOx layer is changed for optimizing microcavity structures. A 10-nm mixed film of Ag and Mg (weight ratio: 1:0.1) was used as a semitransparent cathode.

The relationships between  $y$  chromaticity and current efficiency of the devices using the three dopants were investigated. Figure 11 shows the relationships between  $y$  chromaticity and current efficiency at approximately 1000  $\text{cd}/\text{m}^2$ . In the region of pure-blue chromaticity according to the NTSC standard ( $y = 0.08$ )<sup>27</sup> or the sRGB standard ( $y = 0.06$ ), the device based on BD-05 had a higher current efficiency than the device based on BD-02. This is primarily because the efficiency of energy transfer from the host to BD-05 is higher than that to BD-02. On the other hand, as the  $y$  chromaticity improved, the difference in current efficiency between the devices based on BD-06 and BD-02 increased. For the blue chromaticity of the BT.2020 standard ( $y = 0.046$ ), the current efficiency

of the device based on BD-06 is approximately 1.7 times higher than that of the device based on BD-02. This difference is primarily attributed to shorter emission wavelength of BD-06 than that of BD-02. Thus, it is concluded that BD-06, which has a shorter emission wavelength than BD-02, has advantage for achieving the emission of light with BT.2020 deep-blue chromaticity. Accordingly, BD-05 is an effective dopant for producing the pure-blue chromaticity of the NTSC standard or the sRGB standard, and BD-06 is an effective dopant for the deep-blue chromaticity of the BT.2020 standard.

Next, we estimated the power consumption of panels by assuming the case when OLED panels are fabricated by side-by-side patterning. We assumed the use of our green and red light-emitting materials satisfying the BT.2020 standard, on which we reported previously, for green and red pixels.<sup>28,29</sup> Then, two OLED panels, referring to panel

**TABLE 4** — Estimated characteristics of panel B2 (with a conventional pyrene-based dopant, BD-02) when the panel emits D65 white light at 300  $\text{cd}/\text{m}^2$ .

Chromaticity		Color gamut( $u'$ , $v'$ ) ratio of BT.2020 (%)	Panel luminance ( $\text{cd}/\text{m}^2$ )	Pixel luminance ( $\text{cd}/\text{m}^2$ )	Current efficiency (cd/A)	Voltage (V)	Power consumption ( $\text{mW}/\text{cm}^2$ )
$x$	$y$						
R	0.713	0.287	101	73	3631	36.5	3.97
G	0.182	0.786		209	10470	95.3	3.41
B	0.145	0.046		18	899	3.2	3.19

The power consumptions do not include those of TFT arrays in the estimation.

**TABLE 5** — Estimated characteristics of panel B6 (with one of the novel deep-blue dopant, BD-06) when the panel emits D65 white light at 300  $\text{cd}/\text{m}^2$ .

Chromaticity		Color gamut( $u'$ , $v'$ ) ratio of BT.2020 (%)	Panel luminance ( $\text{cd}/\text{m}^2$ )	Pixel luminance ( $\text{cd}/\text{m}^2$ )	Current efficiency (cd/A)	Voltage (V)	Power consumption ( $\text{mW}/\text{cm}^2$ )
$x$	$y$						
R	0.713	0.287	101	72	3623	36.6	1.96
G	0.182	0.786		210	10497	95.3	1.88
B	0.146	0.045		18	879	5.5	2.46

The power consumptions do not include those of TFT arrays in the estimation.

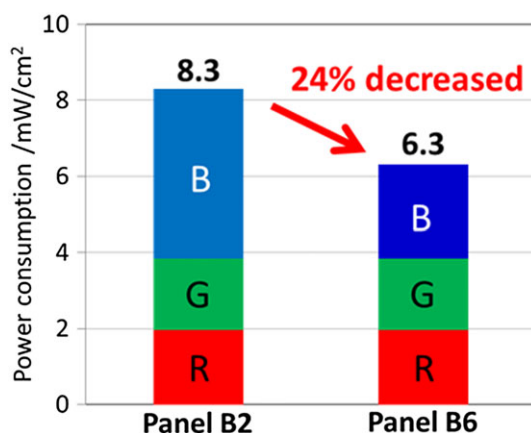


**FIGURE 12** — Estimated power consumptions of panel B2 and panel B6 when the panels emit D65 white light at 300  $\text{cd}/\text{m}^2$ .

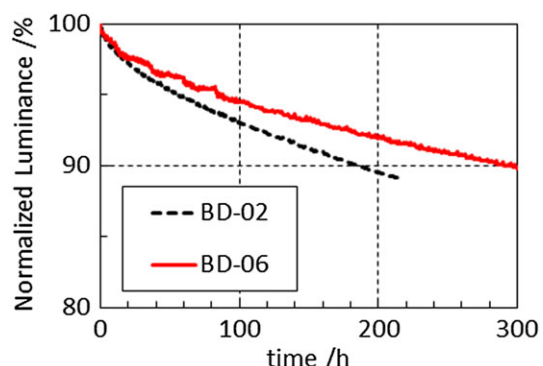


**FIGURE 13** — Normalized luminance decay curves of top-emission devices with BD-02 and BD-06 when driving at the pixel luminance estimated in Tables 4 and 5. Each driving current density is 25.8  $\text{mA}/\text{cm}^2$  for the device with BD-02 and 15.8  $\text{mA}/\text{cm}^2$  for the device with BD-06.

B2 and panel B6, using BD-02 and BD-06 for a blue pixel, respectively, were examined. Tables 4 and 5 show the power consumptions of the panels assumed to display D65 white ( $CIE(x, y) = 0.313, 0.329$ ) over the entire screen (with a size of 4.3 inches and an aspect ratio of 16:9) at a luminance of  $300 \text{ cd/m}^2$  with the aperture ratio of the panel of 15% [5% each for the red, green, and blue (R, G, and B, respectively) subpixels] and light attenuation (e.g., resulting from a circularly polarizing plate) of 60%. The panel luminance of each color (R, G, and B) corresponds to the luminance of the corresponding color component necessary to obtain D65 white color with a luminance of  $300 \text{ cd/m}^2$ . Pixel luminance refers to the intrinsic luminance of a subpixel. Note that the power consumptions do not include those of thin film transistor (TFT) arrays in the above-mentioned estimation.

The BT.2020 area ratio of each panel is larger than 100%. It should be noted that the power consumption of the B subpixel of the panel B6 ( $2.46 \text{ mW/cm}^2$ ) is 45% smaller than the B subpixel of that of the panel B2 ( $4.46 \text{ mW/cm}^2$ ). Accordingly, the power consumption of the whole panel B6 ( $6.30 \text{ mW/cm}^2$ ) was 24% smaller than that of the whole panel B2 ( $8.31 \text{ mW/cm}^2$ ). As one finds out from  $y$  chromaticity vs. current efficiency relationship in Fig. 11, the low-power consumption of the panel B6 is attributed to the improved current efficiency at the chromaticity close to the BT.2020 chromaticity due to the use of BD-06. Figure 12 compares the difference of estimated power consumption of R, G, and B subpixels between panels B2 and B6.

Lastly, the reliabilities of the dopants at the pixel luminances estimated in Tables 4 and 5 were compared. Figure 13 shows the normalized luminance decay curves of top-emission devices with BD-02 and BD-06. The device with BD-06 exhibited less deterioration than the device with BD-02. This marked improvement in reliability is originated from the fact that the efficiency of the device using BD-06 was substantially improved, and thus, its current density at the pixel luminance was reduced.

## 4 Summary

We developed two blue-fluorescent dopants with novel skeletons. These dopants have emission spectra with a short emission wavelength compared with those of conventional pyrene-based dopants. The EQEs of the bottom-emission devices fabricated using the novel dopants (BD-05 and BD-06) were as high as 11.8% and 11.4%, respectively, which are approximately 10% higher than the EQE of 10.7% of the device with the conventional pyrene-based dopant (BD-02). Furthermore, the lifetimes of the devices using the novel dopants were comparable to that of the device with the pyrene-based dopant. The quantitative comparison of the extent of the overlap between the emission spectrum of the host and the molar-absorptivity spectrum of each dopant elucidated that the most important origin of the high

efficiency of the novel dopants is the enhanced rate of energy transfer of singlet excited states from the host to the novel dopants. It was also demonstrated that the current efficiency of the device based on the novel dopant, BD-06, with a microcavity structure is 1.7 times higher than that of the device based on the conventional dopant, BD-02, at the chromaticity close to the BT.2020. As a result, this high current efficiency achieved by BD-06 was estimated to reduce the power consumption of the whole OLED panel by 24%, compared with that of the panel fabricated using BD-02, when assuming that the OLED panels were fabricated by RGB side-by-side patterning.

## Acknowledgments

We are grateful to Professor Emeritus Katsumi Tokumaru for helpful discussion. We also thank Professor Emeritus Tetsuo Tsutsui for his advice and assistance with preparation of this manuscript.

## References

- 1 C. W. Tang *et al.*, "Organic electroluminescent diodes," *Appl. Phys. Lett.*, **51**, 913–915 (1987). <https://doi.org/10.1063/1.98799>.
- 2 ITU-R Recommendation BT.2020-2, "Parameter values for ultra-high definition television systems for production and international programme exchange," (2015)
- 3 ITU-R Recommendation BT.709-5, "Parameter values for the HDTV standards for production and international programme exchange," (2002)
- 4 J. Zhuang *et al.*, "Highly efficient phosphorescent organic light-emitting diodes using a homoleptic iridium(III) complex as a sky-blue dopant," *Org. Electron.*, **14**, 2596–2601 (2013). <https://doi.org/10.1016/j.orgel.2013.06.029>.
- 5 K. Udagawa *et al.*, "Low-driving-voltage blue phosphorescent organic light-emitting devices with external quantum efficiency of 30%," *Adv. Mater.*, **26**, 5062–5066 (2014). <https://doi.org/10.1002/adma.201401621>.
- 6 Y. Yamada *et al.*, "Achievement of blue phosphorescent organic light-emitting diode with high efficiency, low driving voltage, and long lifetime by exciplex-triplet energy transfer technology," *SID Symposium Digest*, **47**, 711–714 (2016).
- 7 A. Endo *et al.*, "Thermally activated delayed fluorescence from  $\text{Sn}(4+)$ -porphyrin complexes and their application to organic light emitting diodes—a novel mechanism for electroluminescence," *Adv. Mater.*, **21**, 4802–4806 (2009). <https://doi.org/10.1002/adma.200900983>.
- 8 Q. S. Zhang *et al.*, "Efficient blue organic light-emitting diodes employing thermally activated delayed fluorescence," *Nat. Photonics*, **8**, 326–332 (2014). <https://doi.org/10.1038/nphoton.2014.12>.
- 9 T. Hatakeyama *et al.*, "Ultrapure blue thermally activated delayed fluorescence molecules: efficient HOMO–LUMO separation by the multiple resonance effect," *Adv. Mater.*, **28**, 2777–2781 (2016). <https://doi.org/10.1002/adma.201505491>.
- 10 D. Y. Kondakov, "Characterization of triplet-triplet annihilation in organic light-emitting diodes based on anthracene derivatives," *J. Appl. Phys.*, **102**, 114504 (2007). <https://doi.org/10.1063/1.2818362>.
- 11 D. Y. Kondakov *et al.*, "Triplet annihilation exceeding spin statistical limit in highly efficient fluorescent organic light-emitting diodes," *J. Appl. Phys.*, **106**, 124510 (2009). <https://doi.org/10.1063/1.3273407>.
- 12 D. Y. Kondakov *et al.*, "Role of triplet-triplet annihilation in highly efficient fluorescent devices," *J. Soc. Inf. Disp.*, **17**, 137 (2009). <https://doi.org/10.1889/JSID17.2.137>.
- 13 N. Hashimoto *et al.*, "Investigation of effect of triplet-triplet annihilation and molecular orientation on external quantum efficiency of ultrahigh-efficiency blue fluorescent device," *SID Symposium Digest*, **47**, 301–304 (2016).
- 14 T. Suzuki *et al.*, "Highly efficient long-life blue fluorescent organic light-emitting diode exhibiting triplet-triplet annihilation effects

enhanced by a novel hole-transporting material,” *Jpn. J. Appl. Phys.*, **53**, 052102 (2014). <https://doi.org/10.7567/JJAP.53.052102>.

- 15 S. Yamazaki and T. Tsutsui, Physics and Technology of Crystalline Oxide Semiconductor CAAC-IGZO: Application to Display, Wiley Series in Display technology, Hoboken, NJ, USA: Wiley (2017), pp. 243–253.
- 16 N. Hashimoto *et al.*, “Long-lived thermally stable blue OLED achieving BT.2020 color gamut,” *SID Symposium Digest*, **48**, 786–789 (2017).
- 17 S. Yamazaki and T. Tsutsui, “*supra* note 15,” , 198–201.
- 18 S. Yamazaki *et al.*, “Method for manufacturing display device,” *US Patent Appl. Publ.* 2005/0197030 (2005).
- 19 H. Ikeda *et al.*, “Low-drive-voltage OLEDs with a buffer layer having molybdenum oxide,” *SID Symposium Digest*, **37**, 923 (2006).
- 20 S. Seo *et al.*, “High-efficient green OLED over 150 lm/W with new P-doped layer exhibiting no optical loss derived from charge transfer complex,” *SID Symposium Digest*, **41**, 148 (2010).
- 21 S. Yamazaki and T. Tsutsui, “*supra* note 15,” , 201–210.
- 22 M. Flämmich *et al.*, “Orientation of emissive dipoles in OLEDs: quantitative in situ analysis,” *Org. Electron.*, **11**, 1039–1046 (2010). <https://doi.org/10.1016/j.orgel.2010.03.002>.
- 23 P. Liehm *et al.*, “Comparing the emissive dipole orientation of two similar phosphorescent green emitter molecules in highly efficient organic light-emitting diodes,” *Appl. Phys. Lett.*, **101**, 253304 (2012). <https://doi.org/10.1063/1.4773188>.
- 24 S. Yamazaki and T. Tsutsui, “*supra* note 15,” , 253–261.
- 25 T. Förster, “Zwischenmolekulare Energiewanderung und Fluoreszenz,” *Ann. Phys.*, **2**, 55–75 (1948). <https://doi.org/10.1002/andp.19484370105>.
- 26 S. Yamazaki and T. Tsutsui, “*supra* note 15,” , 210–214.
- 27 ITU-R Recommendation BT.1700, “Characteristics of composite video signals for conventional analogue television systems,” (2004)
- 28 S. Hosoumi *et al.*, “Ultra-wide color gamut OLED display using a deep-red phosphorescent device with high efficiency, long life, thermal stability, and absolute BT.2020 red chromaticity,” *SID Symposium Digest*, **48**, 13–16 (2017).
- 29 T. Sasaki *et al.*, “A 13.3-inch 8K x 4K 664-ppi 120-Hz 12-bit display with Super-wide Color Gamut for the BT.2020 standard,” *SID Symposium Digest*, **48**, 123–126 (2017).



**Naoaki Hashimoto** received his PhD, ME, and BE degrees in chemistry from the University of Tohoku, Japan, in 2006, 2008, and 2011, respectively. After graduation, he joined Semiconductor Energy Laboratory and has been engaged in R&D of OLED materials and devices.



**Shiho Nomura** graduated from National Institute of Technology, Ube College, Japan, in 2016. After graduation, she joined Semiconductor Energy Laboratory Co., Ltd. Since then, she has been engaged in R&D of OLED.



**Tsunenori Suzuki** received his BS and MS degrees in chemistry from Waseda University, Japan, in 2001 and 2003, respectively. After graduation, he joined Semiconductor Energy Laboratory Co., Ltd. and has been engaged in R&D of OLED materials and devices.



**Harue Nakashima** received her BAg degree from Kyoto Institute of Technology, Japan, in 1999, and MS degree from Kyoto University, Japan, in 2001. After graduation, she joined Semiconductor Energy Laboratory Co., Ltd and has been engaged in R&D of OLED.



**Shogo Uesaka** received his BE degree from University of Fukui, Japan, in 2008 and ME degree from Kanazawa University, Japan, in 2010, respectively. After graduation, he joined Semiconductor Energy Laboratory Co., Ltd. Since then, he has been engaged in R&D of OLED.



**Yusuke Takita** received his BS degrees in chemistry from Hokkaido University, Japan, in 2012 and MS degrees in Chemical Sciences and Engineering from Hokkaido University, Japan, in 2014, respectively. After graduation, he joined Semiconductor Energy Laboratory Co., Ltd. and has been engaged in R&D of OLED devices.



**Kyoko Takeda** received her BE and ME degrees in applied chemistry from the University of Hiroshima, Japan, in 2008 and 2010, respectively. After graduation, she joined Semiconductor Energy Laboratory and has been engaged in R&D of OLED materials and devices.



**Satoshi Seo** received his BE and ME degrees in applied chemistry from the University of Tokyo, Japan, in 1998 and 2000, respectively. After graduation, he joined Semiconductor Energy Laboratory and has been engaged in R&D of OLED materials and devices.



**Shunpei Yamazaki** received the BE, ME, PhD, and honorary degrees from Doshisha University, Japan, in 1965, 1967, 1971, and 2011 respectively. He is the founder and president of Semiconductor Energy Laboratory Co., Ltd. He was awarded Medal with Purple Ribbon by the Japanese Prime Minister's Office for the innovation of MOS LSI element technology in 1997 and was the winner of the Okochi Memorial Technology Prize in 2010. He also received the Medal for Leadership in the Advancement of Ceramic Technology from the American Ceramic Society (ACerS) in 2016. He is

a holder of Guinness World Record under the category of "most patents credited as inventor", for the total of 11 353 patents as of June 2016. He is a life fellow of the Institute of Electrical and Electronics Engineers, Inc., a member of the Japan Society of Applied Physics, a foreign member of the Royal Swedish Academy of Engineering Sciences, and Board of Trustees of Ceramic and Glass Industry Foundation (CGIF), the American Ceramic Society.